Journal of Thermal Science Vol.28, No.4 (2019) 608−620

https://doi.org/10.1007/s11630-019-1136-2 **Article ID: 1003-2169(2019)04-0608-13**

Study on Unstable Characteristics of Centrifugal Pump under Different Cavitation Stages

DONG Liang[1], SHANG Huanhuan[1], ZHAO Yuqi[1], LIU Houlin[1], DAI Cui[2*], WANG Ying[1]

1. Research Center of Fluid Machinery Engineering and Technology, Jiangsu University, Zhenjiang 212013, China
2. School of Energy and Power Engineering, Jiangsu University, Zhenjiang 212013, China

© Science Press, Institute of Engineering Thermophysics, CAS and Springer-Verlag GmbH Germany, part of Springer Nature 2019

Abstract: In order to reveal the regularity of unsteady flow of centrifugal pump under different cavitation stages, a visual closed test-bed is built to collect signals such as the distribution of cavitation bubbles at the impeller inlet and external characteristics, etc. in the process of cavitation of centrifugal pumps. Combined with the shape and distribution of bubbles captured by high-speed photography, the cavitation stage of the centrifugal pump is divided. In addition, the variation of vorticity distribution, pressure pulsation and radial force of centrifugal pump under different cavitation stages are studied using the standard k-ε turbulence model and the Kunz cavitation model. Main contributions are as follows: The cavitation bubbles can absorb the energy of vortex core to a certain extent and increase the volume of vortex core. Cavitation bubbles can also block the flow-path and induce the distortion of the internal flow field, resulting in unstable pressure waves that cause a significant increase in pressure pulsation rate. Besides, with the development of cavitation, the radial force on the impeller tends to remain invariable first and then decrease, and trajectory of the radial force changes from closed to open.

Keywords: centrifugal pump, cavitation development stage, cavitation bubble distribution, pressure pulsation, radial force

1. Introduction

Efficiency, reliability and cavitation are three important indicators to evaluate the performance of the centrifugal pump. Thereinto, cavitation is considered as the "cancer" in the pump field which has not been well solved for a long time [1-3]. The essence of cavitation flow is gas-liquid two-phase turbulent flow, including quite complex mass transfer, momentum transfer and energy exchange between bubbles and water. Cavitation of pump not only has great influence on pump efficiency, but also causes serious damage to materials. The most important research work for cavitation of centrifugal pumps is how to evaluate the state. The conventional energy method to judge the cavitation inception of a centrifugal pump is based on the drop of 3% of the head. It is regrettable that there is a great lag in this method. However, other methods of determining cavitation cannot guide the engineering application as well for the low sensitivity and poor universality. With the development of computer technology and computational fluid mechanics, the method of establishing the relationship between cavitation and the distribution of cavitation flow field, the regulation of the generation and the development of bubbles, etc. by CFD has been widely concerned [4-8].

Tan [9] has studied the internal transient flow of centrifugal pump under cavitation, and found that the motion of cavitation bubbles in impeller presents

Received: Jan 17, 2019 AE: DU Juan Corresponding author: DAI Cui E-mail: daicui@ujs.edu.cn

periodicity, and the dominant frequency of induced pressure pulsation changes from blade frequency to low frequency in comparison with the non-cavitating conditions. MM Athavale [10] carried out numerical simulation of cavitation-flow in hydraulic jet propulsion pump, centrifugal pump and turbopump, etc. by using the Singhal cavitation model. The results show that the occurrence of cavitation is always on the suction surface at the leading edge of blade. Li et al. [11] established a closed loop to analyze the relationship between the cavitation performance and the suction pressure signals. The static parameters used can only capture the critical cavitation condition and cavitation damage condition, whereas they are difficult for the detection of incipient cavitation in the pump. In addition, cavitation produces complex vortex structures inside the flow field, which enhance the interaction between turbulent flow and cavitation [12]. Friedrichs and Kosyna [13] discussed the effects of the cavitation number and the incidence angle of the blade on rotating cavitation through an experimental investigation of two similar centrifugal pump impellers of low specific speed.

The external characteristics of centrifugal pump and the change in the shape of cavitation bubbles attached to the impeller at varied cavitation numbers were conducted by Li et al. [14]. It is pointed out that the size of cavitation bubbles increases with the decrease of cavitation number and so does the decline in performance of a centrifugal pump. The application of the cavitation model has been implemented to investigate the internal relationship between the force of the impeller and cavitation [15]. The obtained results show that the axial force increases with the development of cavitation, however, the radial force changes little with cavitation under rated conditions, instead of reducing in low flow rate. Pouffary et al. [16] analyzed the variations of head and energy conversion process of the centrifugal pump under cavitation conditions, and found that the head decreases with reduction of power and blade load.

It should be noted that cavitating flow is complex multiphase turbulence [17], and the vortex structure can enhance the turbulent intensity of flow field [18]. Thus, the complex vortex structure generated by the cavitating flow contributes to the better interaction between turbulent flow and cavitation bubble [19]. Gopalan and Katz [20] studied enclosed area of the nozzle exit by using Particle Image Velocimetry and high-speed photography system. It is found that the collapse of the vapor cavity in the enclosed area is the main mechanism of vorticity, besides, the hairpin structure vortex generated by collapse of the cavity will dominate the flow in the downstream of the cavitation region. The simulation results of the unsteady flow of cavitation in centrifugal pump show that the cavitation has a pulsating characteristic under off-design conditions. Such phenomenon involves the vortex- induced response and the non-uniform pressure distribution on the volute [21]. Centrifugal pumps easily generate cavitation when running off-design conditions. The development of cavitation has an effect on the load distribution on blade. The head, pressure pulsation and radial force are influenced by the load distribution [22]. In addition, the load distribution on blade also changes the blade angle at the leading edge and affects the cavitation performance of pump [23]. Experimental investigations on pressure pulsation induced by cavitation in double suction centrifugal pumps were carried out by Yao et al. [24]. The results show that the amplitude of pressure pulsation at the shaft frequency and the special low frequency of the impeller increases first and then decreases with the development of cavitation.

Based on the available literatures about cavitation, the researchers were concerned with the following important questions: how to analyze cavitation stages of centrifugal pump, which signal treatment to use (in the frequency or time domain), and which parameter to calculate in order to quantify the degree of erosive cavitation. Few scholars have summarized the characteristics of the unsteady flow of cavitation in centrifugal pump based on a reasonable criterion for cavitation stages. Therefore, the primary work of the paper is to build a visual closed test-bed in order to judge the cavitation stages of centrifugal pump combined with high-speed photography. Then, the most applicable model is selected for the computation of cavitating-flow in centrifugal pump by comparing different turbulence models and cavitation models. Finally, the regularity of distribution for vortex structure, pressure pulsation and radial force distribution on the impeller under different cavitation stages are concentrated on to support the decision of different cavitation stages.

2. Test and Numerical Simulation Strategy

2.1 Test device and object

The test system is mainly composed of a high-speed photographic test system, a high-performance data acquisition system, and an external characteristic test system [25]. The physical diagram of the test system is shown in Fig. 1.

Cavitation in a centrifugal pump firstly occurs on the suction side of impeller blade. For a complete distribution of the cavitation bubble at the inlet of centrifugal pump impeller captured by the high-speed photography camera, a sealed and transparent water tank is connected to the inlet of the pump. The water flows sideways through the water tank, and the high-speed camera is located in front of the water tank to make it face the inlet of the impeller. In addition, a vent hole is arranged on the top of the water tank to facilitate the discharge of gas from the system during water addition

and drainage, so as to maintain the stable pressure in the water tank. In order to not affect the performance of the pump after adding the water tank, and to stabilize the inlet flow state, the tank volume is designed to be 0.1 m^3.

A single-stage single-suction centrifugal pump with a specific speed of 117.3 was used as the research object. The calculation formula of specific speed is as follows:

$$n_s = \frac{3.65 \times n \times Q_d^{1/2}}{H_d^{3/4}} \quad (1)$$

The pump design parameters are Q_d = 40 m^3/h, H_d = 8 m and n = 1450 r/min. The main geometric parameters of the pump are shown in Table 1.

(a) High-speed photography (b) Installation of model pump (c) Water tank

Fig. 1 Physical diagram of the test system

Table 1 The main geometric parameters of the pump

	Parameters	Value
Impeller	Inlet diameter, D_1/mm	90
	Outlet diameter, D_2/mm	170
	Number of blade, Z	6
	Scroll of blade, θ/°	120
	Outlet width, b_2/mm	13.1
Volute	Base diameter, D_3/mm	180
	Inlet width, b_3/mm	32
	Outlet diameter, D_4/mm	80

2.2 Numerical simulation method

UG9.0 is employed to model the three-dimensional fluid of the pump. In order to reduce the influence of the boundary conditions on the internal flow field of the pump, an extension section is added at the inlet of the impeller and the outlet of the volute. Based on ANSYS-ICEM15.0, hexahedral grids are applied to mesh the water body in the computational domain. To avoid the influence of the number of grids on the calculation results, five sets of different grids are used to check the correlation of grid, the judgment basis of which is that the head prediction deviation is less than 1% and the calculation time is taken into account. The test of grid correlation is shown in Table 2.

It can be seen that the predicted value of the head remains basically unchanged after the grid number is greater than 2.29×10^6. Therefore, the fourth grid is selected for numerical calculations. As the test changes the boundary conditions, it is usually chosen to adjust the inlet back pressure through the vacuum pump and regulate the flow through the outlet valve. Therefore, the total pressure inlet and flow outlet boundary conditions are employed in the numerical calculation. Based on the multiple Reference Frames (MRF) model, the impeller is set as a rotation domain and the rest of the components are set as a stationary domain. The dynamic-static interfaces (frozen rotor interface for constant calculation and transient rotor-stator for unsteady calculation) are used between the static and dynamic components. Static-static interfaces are used between the static components. Grids are GGI-compliant and all walls are set as no-slip walls.

The fluid is water with 25°C, and the reference pressure is 0 atm. The rotational speed of the impeller is 1450 r/min. The applicability of different turbulence models is verified respectively, and the results are as following. The stability and convergence rate can be improved through the single-stationary calculation result as the initial value. A homogeneous multinomial flow model is used to simulate the cavitation. The saturated vapor pressure of the fluid is set to 3574 Pa; the inlet volume fraction of the vacuole is 0, and the volume fraction of the liquid is 1. The simulation of the entire cavitation process depends on reducing the total pressure of inlet. Unsteady cavitation calculations are performed

Table 2 The test of grid correlation

Program	Inlet section	Outlet section	Volute	Impeller	Total grids	Head/m
1				2.34×10^5	1.64×10^6	8.54
2				4.82×10^5	1.89×10^6	8.31
3	3.17×10^5	2.67×10^5	8.21×10^5	6.23×10^5	2.03×10^6	8.17
4				8.87×10^5	2.29×10^6	8.14
5				1.05×10^5	2.46×10^6	8.15

on the basis of steady cavitation calculations. The time step was set to Δt=1.1494×10^{-4} s which corresponds to about 1° of the impeller rotation angle. A total of 12 rotation cycles were calculated to ensure stable unsteady data, with a total time step of 0.496 s. The convergence criterion was defined as the root-mean-square residual being below 10^{-5}.

2.3 Calculation model

2.3.1 Turbulence model

Different turbulence models are used to calculate the external characteristics of the pump. The results are shown in Fig. 2.

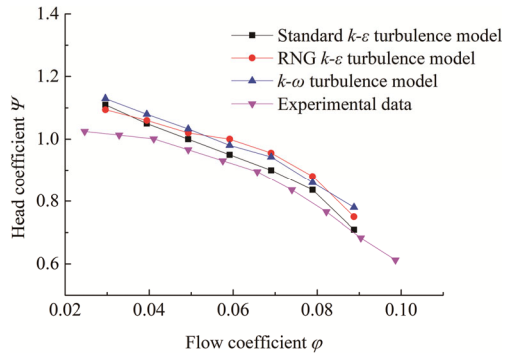

Fig. 2 Comparison between calculated results and experimental values

Head coefficient Ψ:

$$\psi = \frac{H}{u_2^2/2g} \tag{2}$$

Flow coefficient φ:

$$\varphi = \frac{Q}{\pi D_2 b_2 n_2} \tag{3}$$

where, u_2 is the peripheral velocity of the impeller. H is the head. g is the gravity acceleration.

It can be seen from Fig. 2 that the k-ω turbulence model has the largest error under small flow conditions where the flow coefficient φ is 0.02 to 0.04, and the prediction error reaches nearly 20% when φ=0.025. Compared with the other turbulence models, the prediction error is within 8%, but the head-predicted value of the standard k-ε turbulence model is larger than that of the RNG k-ε turbulence model. When the flow coefficient φ is increased to 0.05~0.08, predicted value of the standard k-ε turbulence model is the closest to the test value, and the error is only 2.8%. The error of the RNG k-ε turbulence model increases with the increase of the flow rate. The k-ω turbulence model is more accurate than the RNG k-ε turbulence model. The k-ω turbulence model has the largest error under large flow conditions, while the standard k-ε turbulence model has the smallest predictive value. Comprehensively, the error of the standard k-ε turbulence model is smaller than those of the other two turbulence models over the entire flow range. Therefore, the standard k-ε turbulence model was selected for calculation.

2.3.2 Cavitation model

Different cavitation models have been adopted to calculate the cavitation performance of the model pump under rated conditions. The results of the cavitation curves from calculation and experiment are shown in Fig. 3.

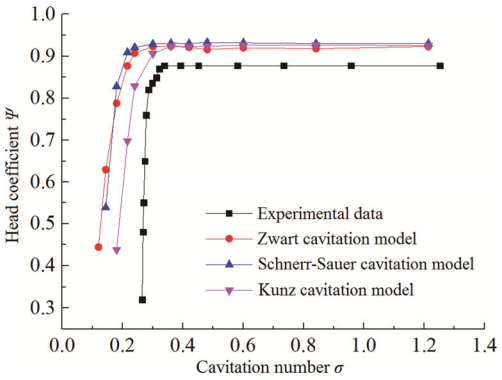

Fig. 3 Comparison between performance curves of different cavitation models and experimental values

Cavitation number σ:

$$\sigma = \frac{p_{\text{in}} - p_{\text{v}}}{0.5\rho_l u_2^2} \tag{4}$$

p_{in} is the static pressure of the pump inlet. p_{v} is the saturated vapor pressure value of the liquid, and takes p_{v} = 3574 Pa. ρ_l is the density of the liquid.

It can be seen from Fig. 3 that the difference in the head coefficient calculated by the different cavitation models is very small in the cavitation number more than 0.4, indicating that the selection of the cavitation model has little effect on the pump characteristics at the non-cavitation stage. When the cavitation number decreases to a certain extent, the head coefficient drops sharply. It can be seen that the result of Kunz cavitation model is closer to the experimental value than those of the Zwart cavitation model and the Schnerr-Sauer cavitation model. When the cavitation number σ=0.27, the head value drops by 3% compared to the non-cavitation stage. Since the Zwart model and the Schnerr-Sauer model are based on the phase change rate expression derived from the vapor-liquid two-term continuity equation, and the final cavitation model is obtained by correcting the phase transition rate based on the generation and collapse of the vacuole. While the Kunz cavitation model considers the generation and the collapse of a vacuole respectively, different methods are used to derive the expression of the mass transfer rate. Besides, the Kunz cavitation model is more suitable for the complex turbulent flow in

centrifugal pumps due to the correlation between the characteristic length, free flow velocity and Reynolds number. Therefore, the Kunz cavitation model is selected to simulate the model pump and study the effect of the whole cavitation process on the internal flow state and external characteristics of the pump.

2.4 Definition of cavitation stage based on high-speed photography

The cavitation flow field at the inlet of the impeller at rated speed and rated flow condition φ = 0.065 is photographed by high-speed photography, and the results under different cavitation numbers are shown in Fig. 4.

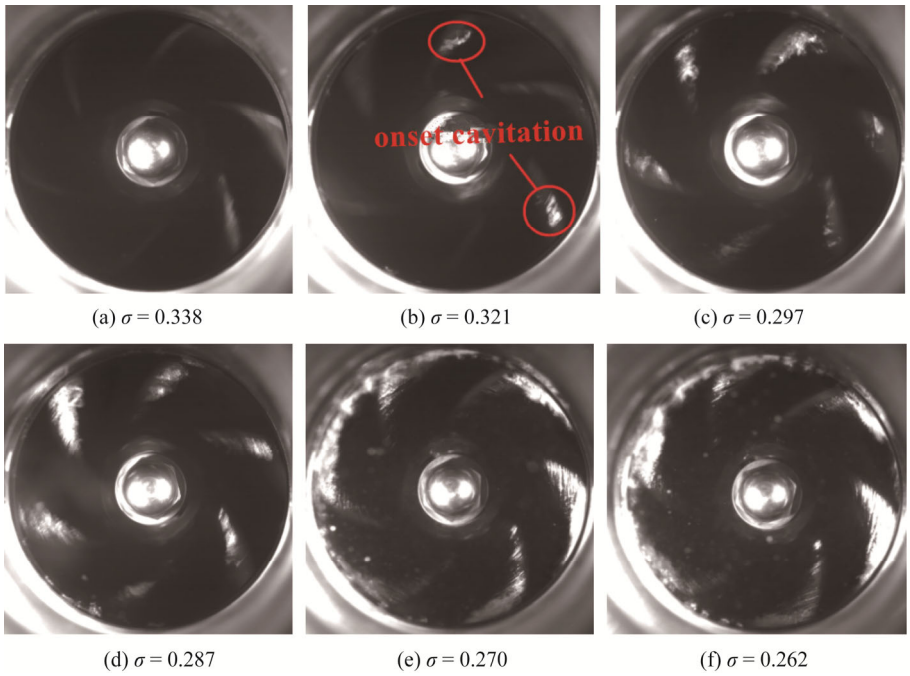

Fig. 4 Test results of high speed photography under different cavitation number in the rated operating state of φ=0.065

As can be seen from Fig. 4, when the cavitation number is 0.338, the cavitation of pump impeller inlet has not been captured. A small amount of bubbles begin to appear at the suction surface of the impeller inlet along with the decrease of cavitation number to 0.321. At this time, the corresponding cavitation number of onset cavitation relying on high-speed photography is taken as the visible cavitation inception. When the cavitation number is 0.297 the head coefficient of cavitation performance curve drops by 3% on account of the statistics of the external characteristic parameters measured by the test. It shows that when the cavitation initially occurs in the pump, the head coefficient will not change significantly, and the hydraulic performance of the pump will not be affected. Then, when the cavitation number is 0.321, the asymmetric structure of the volute and the position of volute tongue play a role in pressure distribution of the flow-path. So bubbles are nonuniformly distributed that the bubbles do not appear on each blade at the same time. Gradually, cavitation is observed on each blade as the cavitation number decreases to 0.297. When the cavitation number is less than 0.27, the bubbles between blades appear to be connected. With the aggravation of cavitation phenomenon, there are a small number of wandering bubbles attached to the surface of the blade. And the area of bubble distribution on the suction surface of the blade at the inlet of the pump is basically unchanged. However, the thickness of the bubble will not be confirmed from such direction.

In a word, taking the rated working conditions as an example, the development process of cavitation on the basis of high-speed photography test can be divided into 4 stages as shown in Fig. 5, non-cavitating stage, onset

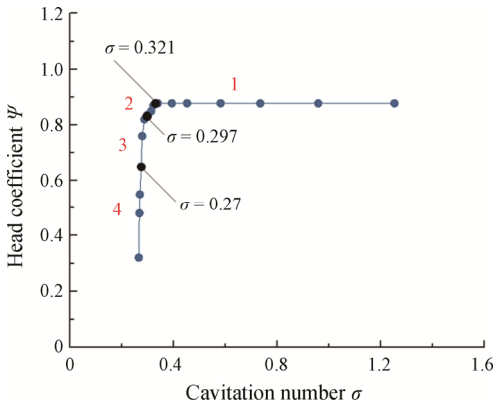

Fig. 5 Schematic diagram of cavitation stage division

cavitation stage, the development cavitation stage, and severe cavitation stage.

Non-cavitating stage. When the cavitation number is higher than 0.321, the head coefficient in the cavitation performance curve does not change, and high-speed photography does not capture cavitation bubbles. When the cavitation number decreases to 0.321, the head coefficient has not changed yet, and high-speed photography captures a small amount of bubbles on the suction surface at the inlet of the blade.

Onset cavitation stage. With the gradual increase of the cavitation bubbles, cavitation gradually affects the hydraulic performance of the pump. When the cavitation number reduces to 0.297, in other words, the head coefficient of cavitation performance curve decreases by 3%, more vacuoles appear in the impeller inlet.

The development cavitation stage. When the number of cavitation drops to 0.27, the head coefficient of the cavitation performance curve shows a sharp decline. And the extreme value of cavitation at the inlet of impeller is observed by high-speed photography.

Severe cavitation stage. When the cavitation number is less than 0.27, the increase of vacuole gradually blocks the inlet of the impeller.

3. Effect of Cavitation on Internal Flow

The condition that the local pressure of the centrifugal pump is lower than the saturated vapor pressure of the medium at certain temperature leads to the occurrence of cavitation. The choice of cavitation number ensures that the variation rule of the cavitation process can be reflected and the different stages can be accurately divided. At pump operating mode with φ = 0.065, the cavitation number 0.37 corresponds to non-cavitating stage, the cavitation number 0.31 corresponds to onset cavitation stage, the cavitation number 0.28 corresponds to the development cavitation stage, and the cavitation number 0.26 corresponds to severe cavitation stage.

3.1 Effect of cavitation on cavitating flow

The concentrated low-pressure area is easy to occur in the pump, especially at the inlet of the impeller. The reason for the phenomenon is that separation of flow, incoming flow, back-flow, and impingement flow etc. causes a considerable loss in energy. Furthermore, the suction surface of the blade shows a more obvious low-pressure area than the pressure surface because of the different work characteristics of the blade, and it is usually considered as locations liable to cavitation. At rated flow, the distribution of the iso-surface with the phase volume fraction of gas is 0.5 under different cavitation stages of the pump is shown in Fig. 6. The cavitation can be clearly divided into 3 regions: bubble generation (blue region), bubble development (green region) and bubble collapse (red region). The generation and development of cavitation affect not only the internal flow of the pump, but also the operating characteristics of the pump. As you can see from Fig. 6, the cavitation is centrally symmetric on the whole, which firstly happens

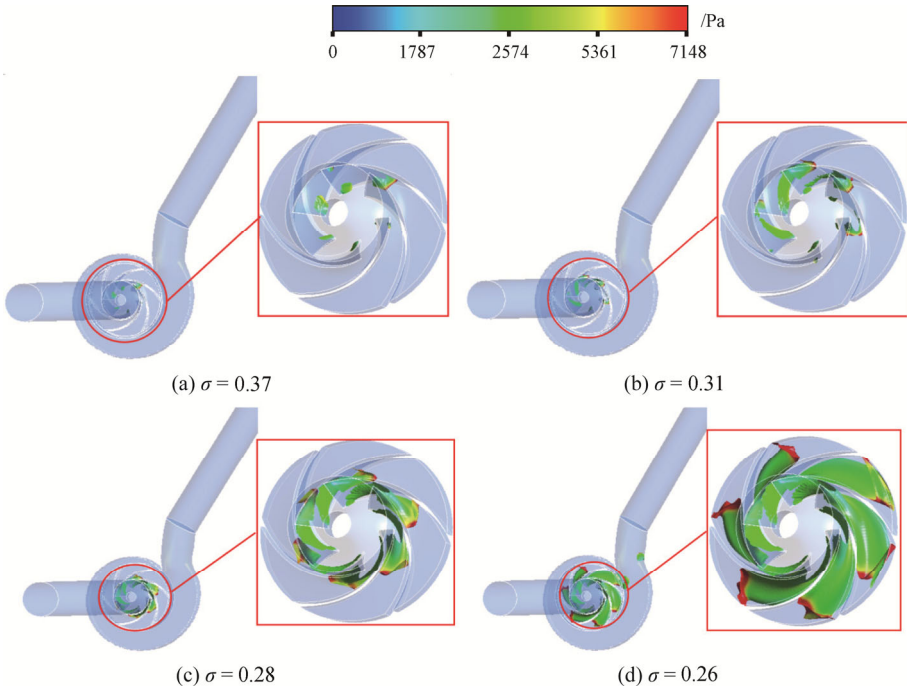

Fig. 6 Cavitation region corresponding to cavitation number in rated flow

on the suction surface near the inlet of the impeller.

With the development of cavitation, the scope of cavitation gradually expands and cavitation extends from the suction surface to the pressure surface. Separation of flow induced by cavitation in the inlet of the impeller triggers the blockage of the flow-path and affects the hydraulic performance of the pump. The region of bubble generation remains unchanged, and the bubble collapse region transfers out of the flow-path of the impeller. When the cavitation develops to a certain extent, it will show a distinctly unstable flow characteristic. The uniformity of cavitation is increased for the influence of the volute pressurized water chamber. Thanks to the small area of bubble collapse in the impeller passage near volute tongue, a great number of cavitation bubbles enter the volute, leading to the appearance of the bubble collapse in the extension section of the export. What's more, slight cavitation will emerge at the leading edge of impeller inlet following the deterioration of cavitation. That is because severe cavitation exacerbates the unsteady flow in the inlet of the impeller blade and the blockage of the flow-path enhances the back-flow vortex, the large static pressure loss is produced at the leading edge of the impeller inlet.

3.2 Effect of cavitation on vortex structure

Cavitation of pump is always accompanied by a strong vortex flow, which will inevitably affect the internal flow of the pump. Therefore, it is necessary to analyze the vortex structure in the centrifugal pump under a cavitating flow condition. *Q-Criterion* [26] is the most common discriminate criterion of vortex for its explicit physical meaning. *Q-Criterion* determines the vorticity of the fluid micromass according to the virtual part of the complex number of the fluid velocity gradient tensor. The rotation strength of fluid micromass strengthens with the increase of *Q-value* and the greater the *Q-value*, the greater the vortex intensity. Fig. 7 shows the variation distribution of the vortex core region with the *Q-value* under different cavitation stages. Different colors represent the velocity distribution in the vortex core region and the *Q-value* represents the dimensionless quantity of the *Q-Criterion*/Q_{max} ranging between 0~1 in Fig. 7.

(1) In non-cavitating stage, the change of *Q-value* has great influence on the vortex core distribution in the flow-path of impeller. When the *Q-value* is small, the vortex core is produced by the suction surface of the impeller. And the suction surface at the outlet of the impeller is the high-speed region of the vortex core, while the vortex core area in the impeller is small while the vortex core area in the impeller is small. The vortex core is developed to the pressure surface and the vortex core area gradually expands in pace with the growth of

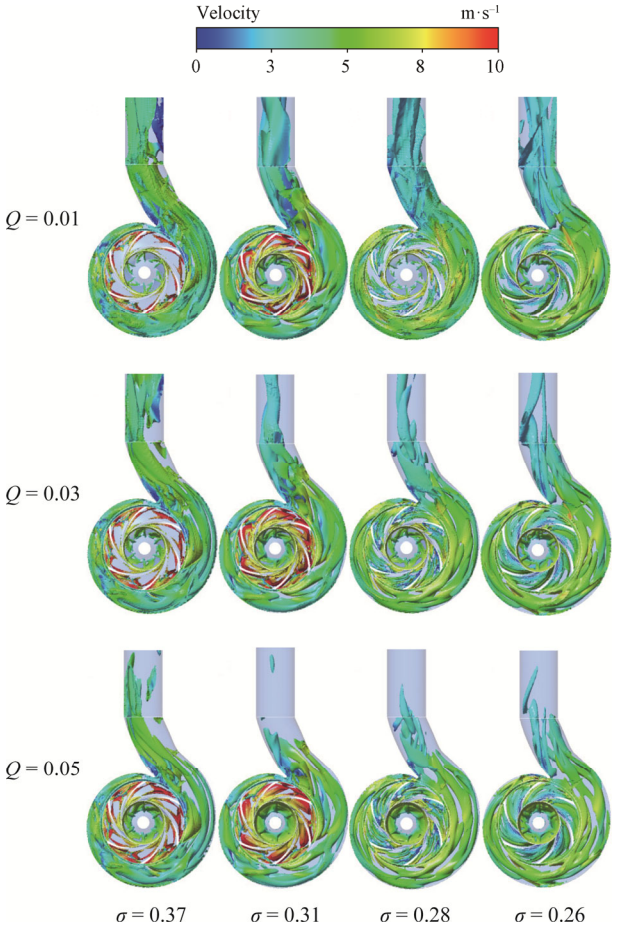

Fig. 7 Regional distribution of vortex core with different *Q-values* under different cavitation stages in rated flow

Q-value. The vortex core region develops mainly from the inlet of impeller, soon extends to the flow-path, besides, the distribution of vortex core is obvious in the pressurized water chamber.

(2) After the occurrence of cavitation, the shape and location of vortex core in impeller channel are not significantly affected by *Q-value*, but only slightly different at the outlet and its extension of volute. Under different cavitation stages, the high-intensity vortex in the flow field is mainly concentrated in the rotation region and there is a large energy loss at the vortex core.

(3) At onset cavitation stage, the velocity gradient of the vortex core in the impeller is lower than that in non-cavitating stage and the high-speed region turns from the blade attachment area to the whole flow-path. The reason is that cavitation accelerates the energy exchange in the internal flow of the impeller and evens the velocity of the cavitation. The trend is becoming more apparent with the further development of cavitation.

(4) Cavitation continues to develop into severe

cavitation stage; the cavitation bubble absorbs the energy of the vortex core and weakens the vortex strength. Finally, the high-speed region of vortex core in the impeller is no longer obvious. Instead, a clear low-speed region appears on the suction surface and further shifts to the pressure surface.

The volume contained in the iso-surface of the vortex core is extracted based on the *Q-Criterion*, then it is used to measure the effect of vortex motion on pump operation. The volume distribution of vortex structure can explain the difference in pump efficiency, that is, the cavitation leads to a certain increase of vortex, and it partly affects the operation efficiency of the centrifugal pump. The volume of vortex core corresponding to various *Q-Criterion* levels under different cavitation stages is shown in Fig. 8.

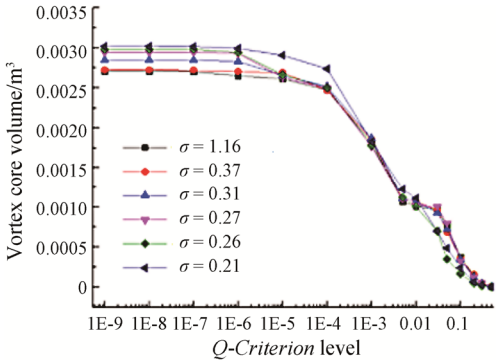

Fig. 8 Variation of vortex core volume with different *Q-values* under different cavitation stages in rated conditions

As can be seen from the picture, the volume distribution curve of the vortex core under different cavitation stages shows the same change regularity. The volume of vortex core decreases with the increase of *Q-value*, and eventually it tends to fixed value. It varies slightly under different cavitation stages with high *Q-value*. It is larger in non-cavitating stage and the development cavitation stage, but has a downward trend after the cavitation worsens. However, in the region with lower Q value, the volume of vortex core increases significantly with the development of cavitation.

4. Effect of Cavitation on Unsteady Force

4.1 Effect of cavitation on pressure pulsation

In order to study the effect of cavitation on pressure pulsation at different locations, 36 monitoring points are arranged clockwise every 10 degrees on the outer edge of the impeller. Fig. 9 is the layout of the monitoring points.

In rated flow condition, the time domain data of pressure pulsation in the last period are processed when

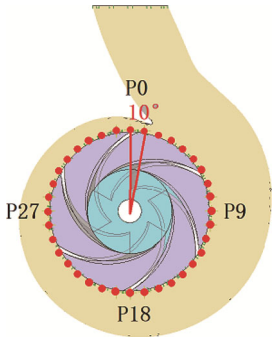

Fig. 9 Schematic diagram of monitoring points for pressure pulsation

the unsteady calculation of cavitation tends to be stable. The pressure pulsation is dimensionless according to formula (5) and is in the form of pressure pulsation coefficient C_p.

$$C_p = \frac{p_i - \frac{1}{n}\sum_{i=1}^{n} p_i}{\frac{1}{2}\rho u_2} \tag{5}$$

In the formula, p_i represents the pressure value calculated at the unit time step; ρ is the density of fluid medium; u is the circumferential velocity of the impeller.

Fig. 10 reveals the time domain of pressure pulsation coefficient under different cavitation stages. It can be seen from Fig. 10 that clear periodic variation is expressed by the coefficient distribution of pressure pulsation at various monitoring points in non-cavitating stage with the cavitation number is 0.37. A fixed monitoring point in a cycle shows 6 peaks and 6 troughs corresponding to the number of blades. It is the same with different monitoring points at different time. To compare the different monitoring points, it is concluded that the extreme value of pressure pulsation coefficient appears between the points of 30~0 and 0~5 near the tongue. The reason is that the pressure pulsation in the pump caused by the rotor-stator interaction of the rotating impeller and the static volute tongue is mainly concentrated on the tongue. In addition, there will be a sub-peak near the crest, and its value will gradually decrease with the development of cavitation. When the cavitation number is 0.31 (onset cavitation stage), a small amount of bubbles has been born in the impeller, but the output of bubbles is too little to have a significant impact on the internal flow. The internal flow and the sharp attenuation of high-frequency energy are not affected by the tiny amount of bubbles, which makes a small change in the pressure pulsation coefficient. In the stage of cavitation development, large cavitation areas will form in the impeller. The large-scale cavitation bubbles not only obstruct impeller flow-path, induce distortion of internal flow and shape unstable pressure wave, but also

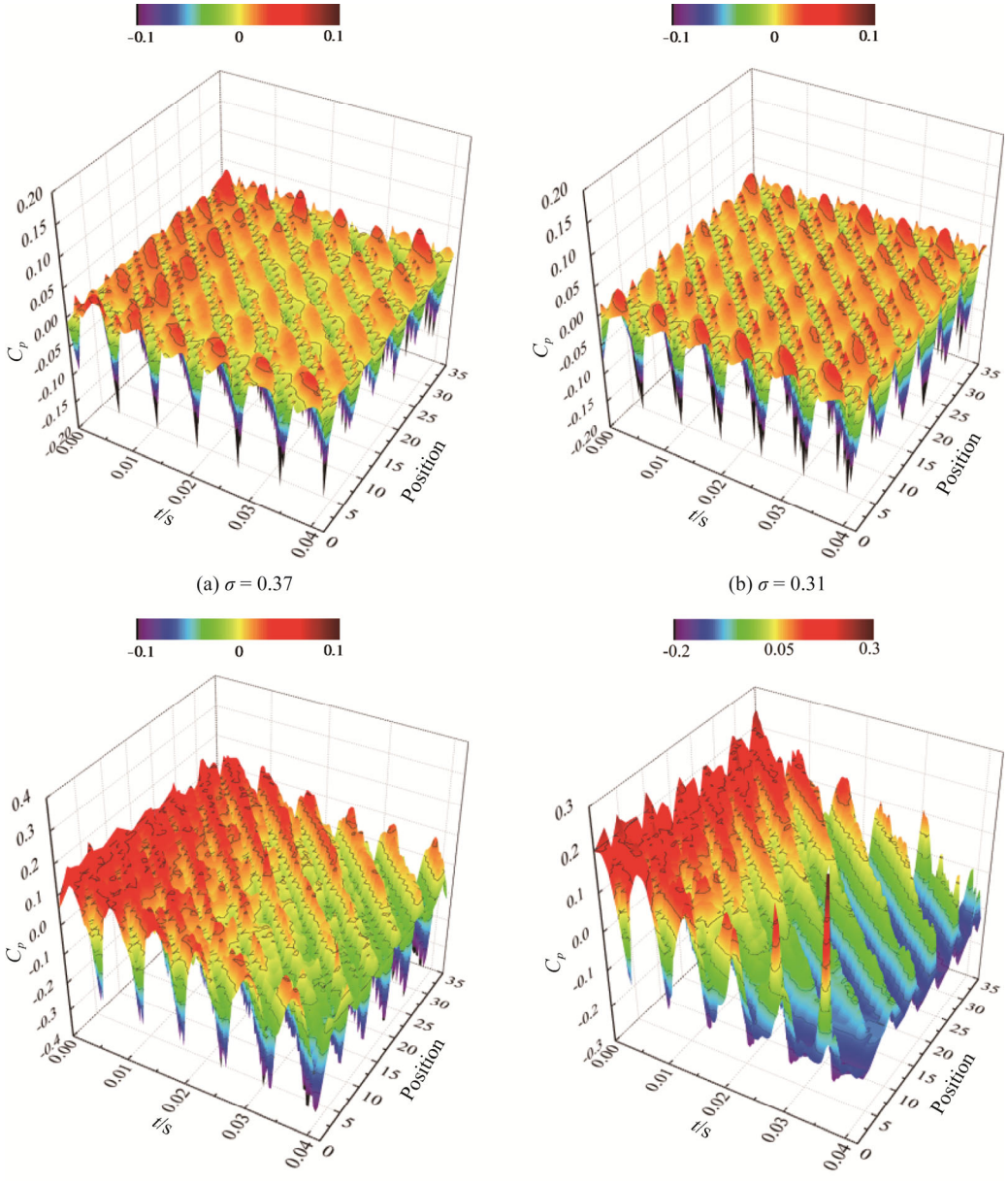

Fig. 10 Influence of cavitation on time domain distribution of pressure pulsation

cause the rate of change of pressure pulsation markedly increased. The above phenomena affect the working stability of the pump and induce large vibration noise. In the period of severe cavitation, the pressure pulsation does not change evenly with time in a cycle of rotation of the impeller. The instability of the pressure pulsation is not reflected in the increase of the pressure pulse coefficient against a fixed monitoring point and its increase of the change rate, but in the more and more obvious fluctuation of the mean of the pressure pulsation in the pump with the development of the cavitation.

In order to analyze the frequency spectrum of the pressure pulsation, Fourier transformation is carried out for the sample data of the 6 subsequent stable periods based on the pressure pulsation of different monitoring points. After combining it with the analysis of pressure pulsation coefficient under different cavitation stages, the influence of cavitation on the energy of pressure pulsation is obtained. Based on the above work, the effect of cavitation on pressure pulsation is mainly reflected in the component of shaft frequency, blade frequency and its frequency doubling, instead of the trend of distribution from high frequency to low frequency. For the purpose of exploring the effect of cavitation on the eigenfrequency of pressure pulsation, the relationship between shaft frequency in 1 to 3 times and different

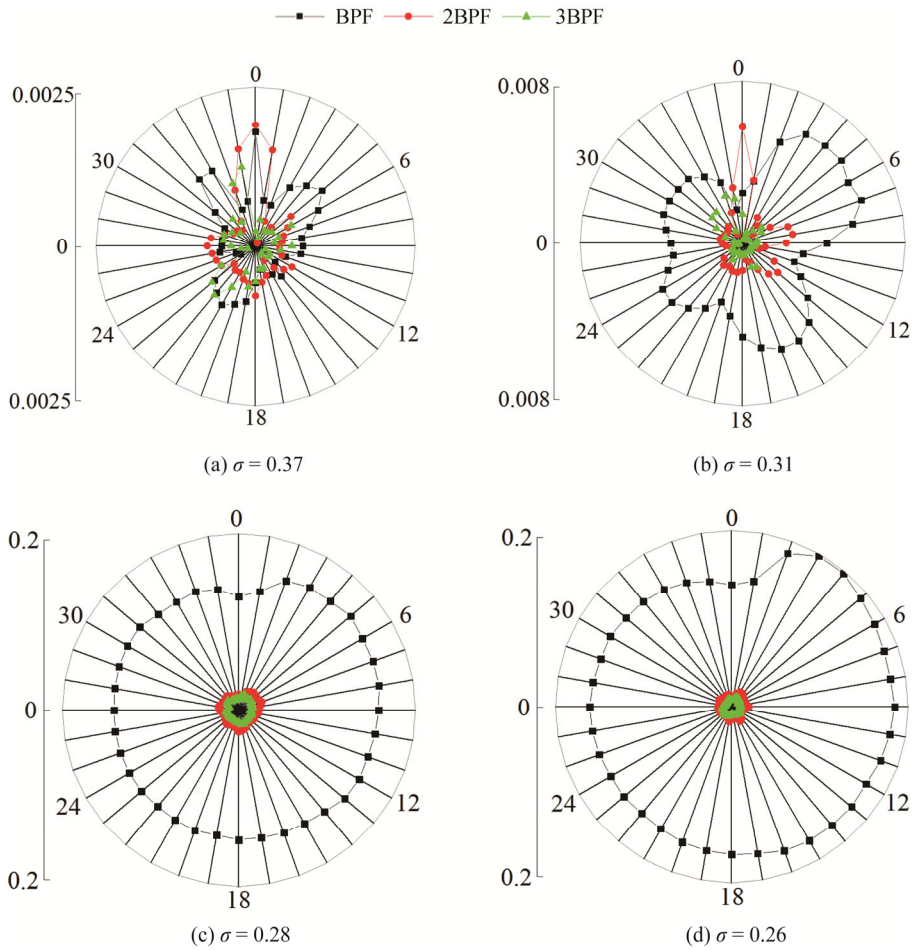

Fig. 11 Influence of cavitation on shaft frequency and frequency doubling distribution of pressure pulsation

monitoring points under different cavitation numbers is calculated. As shown in Fig. 11, the ordinate represents the dimensionless pressure pulsation coefficient.

It can be seen from Fig. 11 that there are no obvious regularities of distribution of shaft frequency and frequency doubling at non-cavitating stage along with small magnitude of the pulsation and low energy. At onset cavitation stage, distribution of shaft frequency and frequency doubling have a greater degree of change compared with those at non-cavitation stage, but magnitude of the pulsation remains small. It shows that the development of cavitation has little influence on the shaft frequency pulsation. At the development cavitation stage, the shaft frequency component increases obviously, and a small peak appears between the 35~4 monitoring points. At severe cavitation stage, shaft frequency component is significantly higher than that of the frequency doubling component, moreover, the distribution of shaft frequency component comes into being a shape similar to volute. It reaches the highest peak between the 2~4 monitoring points and decreases along the monitoring points number to the minimum at the 0 point. The foregoing phenomenons are regularities of distribution of shaft frequency pulsation when cavitation develops to a relative severity. From the whole process of cavitation, the variation of frequency doubling is also considerably complex. Nevertheless, it can be seen that the shaft frequency remains the dominant frequency because its energy is larger than that of the frequency doubling component.

4.2 Effect of cavitation on radial force

The force components F_x and F_y of all the solid walls in the impeller area (the blade, the front cover plate and the rear cover plate) in two axial perpendicular directions x and y are calculated to solve the radial force F of the impeller; θ_F represents the direction angle of force. The formulas are as follows:

$$F = \left(F_x^2 + F_y^2\right)^{\frac{1}{2}} \tag{6}$$

$$\theta_F = \arctan\left(F_y / F_x\right) \tag{7}$$

On the basis of the formulas, the radial force and the direction angle of the impeller in one period of rotation

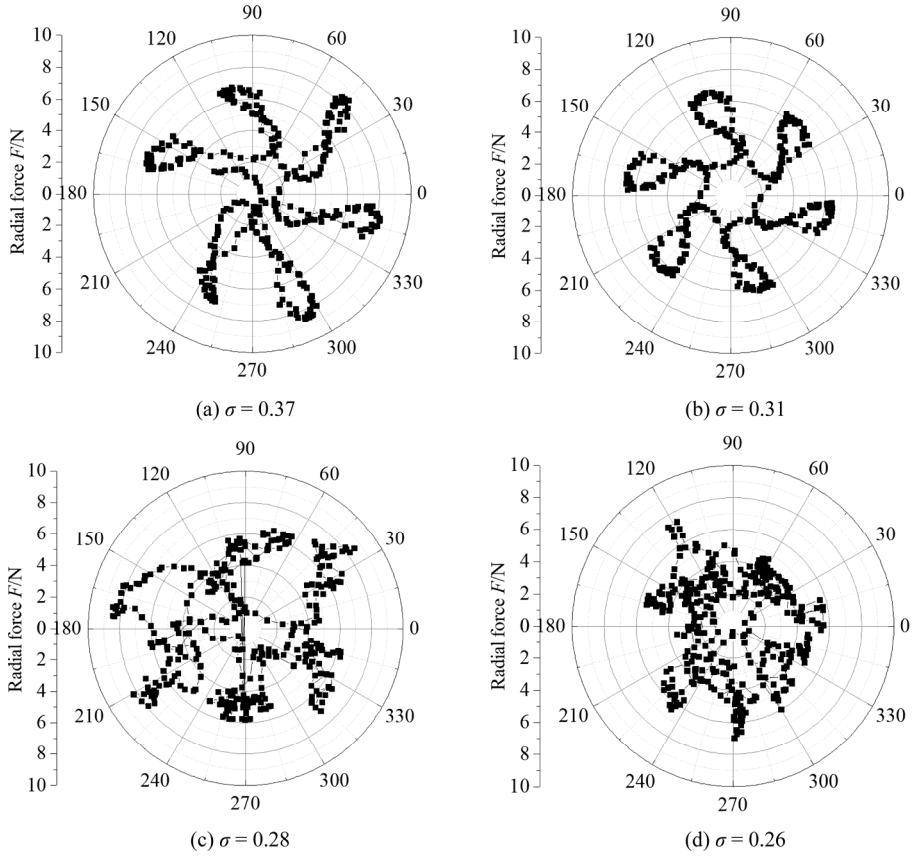

Fig. 12 Polar diagram of radial force on impeller under different cavitation stages

corresponding to the cavitation number under different cavitation stages are calculated. The polar coordinates of the radial force of the impeller under different cavitation stages are shown in Fig. 12.

As can be seen from the above picture, in non-cavitating stage when cavitation number is 0.37, the distribution of radial force shows 6 peaks in the circumference consistent with the number of impeller blades. Further, large radial force is produced on the impeller. In view of the effect of the tongue, when water flows from the spiral section of the pressurized-water chamber into the diffuser, it partly forms vortex to block flow-path. The rest of the water is forced to flow back to the nearest flow-path through the tongue. It induces a low-pressure vortex near the tongue, causes the pressure of this flow-path to be significantly lower than that of other flow-path, and finally results in serious asymmetry of the flow structure.

At onset cavitation stage, the expansion of the cavitation area effectively reduces the differential pressure between the flow-path near the tongue and other flow-path as the pressure of pump suction decreases. It improves the symmetry of the pressure distribution at the outlet of the whole flow-path. Therefore, there is better symmetry of the pressure distribution at the outlet of the impeller and smaller radial force than that in non-cavitating stage. When the cavitation number is reduced to 0.28 with the development of cavitation, the radial force becomes irregular and its trajectory goes into unclosed. The reasons for the result are as follows, when the flow path of the impeller is partially blocked, the medium between the front cover plate and the rear cover plate is not only liquid but also bubbles. The bubbles destroy the symmetry of single-phase flow field and make the force of the impeller unbalanced. So the periodicity and symmetry of the change of the radial force are breached when the impeller rotates, and the distribution of the peak value does not completely correspond to the number of blades. In addition, the effective cross section of flow-path is reduced by the crowding-out effect of cavitation bubbles. The velocity of the fluid in the non-clogged flow-path of the blade increases significantly and acts on the angle of attack at the inlet of the runner. The interaction between adjacent flow-paths of blade will be continuously transmitted resulting in an unclosed state in radial trajectory of one circle. At the stage of severe cavitation, the radial force is further weakened due to the more severity of the blockage of the flow-path by cavitation bubbles.

With the development of cavitation, radial force first

remains invariable and then declines. What's more, the production of bubbles decreases the fluid-flow in the impeller and increases current velocity at the outlet of the impeller. The reduction of current velocity in the volute combined with the above phenomenon causes the result that the fluid impinges on and mixes with the fluid in the volute instead of flowing smoothly from the impeller to the volute. It is a trigger for raising the fluid pressure in the volute. In virtue of the increase of the fluid pressure, the radial force is counteracted partially and dropped.

5. Conclusions

Combined with high-speed photography and performance test, the cavitation in centrifugal pump is divided into four stages. The standard k-ε turbulence model and Kunz cavitation model have higher accuracy in cavitation simulation of centrifugal pump.

(1) Under different cavitation stages, the high-intensity vortex in the internal flow mainly concentrates in the rotating region. The velocity gradient of vortex core in impeller at onset cavitation stage is smaller than non-cavitating stage. With the development of cavitation, the high-speed region of vortex core gradually spreads from the region attached of the blade to the whole flow-path. When the cavitation phenomenon is further aggravated, low velocity zone obviously appears on the suction surface and further shifts to the pressure surface.

(2) At onset cavitation stage, the production of cavitation bubbles is too small to affect the internal flow of the pump. At the same time, the rapid attenuation of high-frequency energy makes the amplitude of pressure pulsation coefficient smaller than the non-cavitating stage. With the development of cavitation, bubbles will block the flow-path and form unstable pressure waves, resulting in a significant raise in the change rate of pressure pulsation. Besides, the shaft frequency remains the main frequency, and its value increases obviously, although the regulation of shaft frequency and doubling frequency is quite complicated.

(3) At non-cavitating stage and onset cavitation stage, the distribution of the radial force corresponds to the number of impeller blades. Moreover, the radial force is smaller at onset cavitation stage than at non-cavitating stage. The trajectory of radial force is no longer closed with the further development of cavitation. In general, radial force has no definite regularity except for a decreasing tendency.

(4) The limitation of numerical calculation models and test signal acquisition equipment results in some certain error in cavitation flow field calculation. In the future, we can study and explore the accurate method of cavitation flow simulation and acquisition and processing of cavitation signal.

Acknowledgement

This work was supported by the National Key Research and Development Program of China (2017YFC0804107), National Natural Science Foundation of China (No. 51879122, 51779106, 51509111), the association innovation fund of production, learning, and research (BY2016072-01), Zhenjiang key research and development plan (GY2017001, GY2018025), the Open Research Subject of Key Laboratory of Fluid and Power Machinery, Ministry of Education, Xihua University (szjj2015-017, szjj2017-094, szjj2016-068), Sichuan Provincial Key Lab of Process Equipment and Control (GK201614, GK201816), the Advanced Talent Foundation of Jiangsu University (15JDG052) and a project funded by the Priority Academic Program Development of Jiangsu Higher Education Institutions (PAPD), Jiangsu top six talent summit project (GDZB-017).

References

[1] Li Y.Q., Yuan S.W., Lai H.X., Numerical study of unsteady flows with cavitation in a high-speed micro centrifugal pump. Journal of Thermal Science, 2017, 26(01): 18–24.

[2] Zhang N., Yang M.G., Gao B., Li Z., Vibration characteristics induced by cavitation in a centrifugal pump with slope volute. Shock and Vibration, 2015, 2015: 1–10.

[3] Huang B., Wu Q., Wang G.Y., Research status and progress of unstable cavitating flow. Journal of Irrigation and Drainage Machinery Engineering, 2018, 36(01): 1–14. (in Chinese).

[4] Lei T., Shan Z.B., Liang C.S., et al, Numerical simulation of unsteady cavitation flow in a centrifugal pump at off-design conditions. Proceedings of the Institution of Mechanical Engineers, Part C: Journal of Mechanical Engineering Science, 2014, 228(11): 1994–2006.

[5] Li X.J., Jiang Z.W., Zhu Z.C., et al, Entropy generation analysis for the cavitating head-drop characteristic of a centrifugal pump. Proceedings of the Institution of Mechanical Engineers, Part C: Journal of Mechanical Engineering Science, 2018: 095440621775345.

[6] Dong L., Zhao Y.Q., Dai C., Wang Y., Research on cavitation acoustic characteristics of centrifugal pump based on fluid-acoustic field coupling method. Advances in Mechanical Engineering, 2018, 10(5): 1-13.

[7] Li Q.F., Liu C., Wang Y.K., Cavitation characteristics of pump-turbine under partial load. Journal of Drainage and Irrigation Machinery Engineering, 2017, 35(08): 680–684. (in Chinese).

[8] Kang J.Y., Zhu R.S., et al, The influence of impeller

geometric parameters on fracture cavitation performance in centrifugal pumps. Journal of Drainage and Irrigation Machinery Engineering, 2018, 36(02): 111–117. (in Chinese).

[9] Tan L., Zhu B.S., Wang Y.C., et al, Numerical study on characteristics of unsteady flow in a centrifugal pump volute at partial load condition. Engineering Computations, 2015, 32(6): 1549–1566.

[10] Athavale M.M., Li H.Y., Yu J., et al, Application of the full cavitation model to pumps and inducers. International Journal of Rotating Machinery, 2014, 8(1): 45–56.

[11] Li X.J., Yu B.X., Ji Y.C., Lu J.X., Yuan S.Q., et al, Statistical characteristics of suction pressure signals for a centrifugal pump under cavitating conditions. Journal of Thermal Science, 2017(26): 47–53.

[12] Belahadji B., Franc P., Michel M., Cavitation in the rotational structures of a turbulent wake. Journal of Fluid Mechanics, 1995, 287: 383–403.

[13] Friedrichs J., Kosyna G., Rotating cavitation in a centrifugal pump impeller of low specific speed. Journal of Fluids Engineering, 2002, 124(2): 356–362.

[14] Li J., Liu L.J., Li G.J., et al, Numerical study on the effect of cavitation number on the hydraulic performance of centrifugal pumps. Journal of Engineering Thermophysics, 2010, V31(5): 773–776. (in Chinese).

[15] He M., Wang C.C., Li X.Q., Study on impeller force characteristics of cavitation flow field in centrifugal pump. General Machinery, 2017(08): 79–83. (in Chinese).

[16] Pouffary B., Fortes-Patella R., Roboud J., et al, Numerical simulation of 3D cavitating flows: analysis of cavitation head drop in turbomachinery. ASME Journal of Fluids Engineering, 2008, 130, p.061301.

[17] Li C.Y., Ceccio S.L., Interaction of single travelling bubbles with the boundary layer and attached cavitation. Journal of Fluid Mechanics, 1996, 322: 329–353.

[18] Arakeri V.H., Acosta A.J., Viscous effects in the inception of cavitation on axisymmetric bodies. Journal of Fluids Engineering, 1973, 95(4): 519–527.

[19] Belahadji B., Franc P., Michel M., Cavitation in the rotational structures of a turbulent wake. Journal of Fluid Mechanics, 1995, 287: 383–403.

[20] Gopalan S., Katz J., Flow structure and modeling issues in the closure region of attached cavitation. Physics of Fluids, 2000, 12(4): 3414–3431.

[21] Meng L., He M., Zhou L., et al., Influence of impeller-tongue interaction on the unsteady cavitation behavior in a centrifugal pump. Engineering Computations, 2016, 33(1): 171–183.

[22] Li X., Gao P., Zhu Z., et al, Effect of the blade loading distribution on hydrodynamic performance of a centrifugal pump with cylindrical blades. Journal of Mechanical Science & Technology, 2018, 32(3): 1161–1170.

[23] Huang R.F., Luo X.W., Ji B., et al., Multi-objective optimization of a mixed-flow pump impeller using modified NSGA-II algorithm. Science China Technological Sciences, 2015, 58(12): 2122–2130.

[24] Yao Z.F., Wang F.J., Xiao R.F., et al., Experimental investigation of pressure instabilities affected by cavitation for a double-suction centrifugal pump. IOP Conference Series: Earth and Environmental Science, 2012, 15(6): 062040.

[25] Dong L., Zhao Y.Q., Liu H.L., Dai C., Vladimirovich Gradov D, Wang Y., The effect of front streamline wrapping angle variation in a super-low specific speed centrifugal pump. Proceedings of the Institution of Mechanical Engineers, Part C: Journal of Mechanical Engineering Science, 2018: 095440621877260.

[26] Hunt J.C.R., Wray A.A., Moin P., Eddies, stream, and convergence zones in turbulent flows. Studying Turbulence Using Numerical Simulation Databases. Studying Turbulence Using Numerical Simulation Databases, 2, 1988.